Molecular Insights into the Differential Dynamics of SARS-CoV-2 Variants of Concern (VOC)

Nabanita Mandal[a] , Aditya K. Padhi[b] and Soumya Lipsa Rath[a]*

[a]National Institute of Technology, Warangal, Telangana, 506004, India

[b]Laboratory for Structural Bioinformatics, Center for Biosystems Dynamics Research, RIKEN, 1-7-22 Suehiro, Tsurumi, Yokohama, Kanagawa 230-0045, Japan.

* Corresponding Author Email: slrath@nitw.ac.in

Abstract

Severe Acute Respiratory Syndrome Coronavirus 2 (SARS-CoV-2) has affected the lives and livelihood of millions of individuals around the world. It has mutated several times after its first inception, with an estimated two mutations occurring every month. Although we have been successful in developing vaccines against the virus, emergence of variants has enabled it to escape therapy. Few of the generated variants are also reported to be more infectious than the Wild-type. The World Health Organization (WHO) has prioritized the variants into Variants of Concern (VOC) and Variants of Interest (VOI) to focus on the variants that pose a threat to public health. In this study, we compare the structural and dynamic attributes of all the RBD/ACE2 complexes for the reported VOCs, namely, Alpha, Beta, Gamma, and Delta through atomistic simulations. Results indicated that the orientation and binding energies of the VOCs were different from the Wild-type. Specifically, we observed that the Receptor Binding Domain (RBD) in B.1.351 (Beta) and B.1.617.2 (Delta) underwent a relative rotation to make the complex more compact. Protein dynamics, however, show that their fluctuations were similar to the Wild-type. It was also reflected in the calculation of the total interaction energies. Overall, it was observed that electrostatic interactions play a major role in the formation of the complexes. Detailed residue level energetics revealed that the most prominent changes in interaction energies were seen particularly at the mutated residues which were present at RBD/ACE2 interface. We found that B.1.167.2 (Delta) is one of the most tightly bound variants of SARS-CoV-2 with dynamics similar to Wild-type. High binding affinity of RBD towards ACE2 is indicative of an increase in the viral infectivity.

Therefore, the intrinsic details presented in this study would be useful for the design and development of effective therapeutic strategies for the emerging variants of the virus.

Keywords: VOCs, Delta, SARS-CoV-2, Molecular Dynamics, RBD, ACE2

Introduction

Severe Acute Respiratory Syndrome Coronavirus 2 (SARS-CoV-2), is one of the largest known RNA viruses with a single-stranded RNA ranging between 26,000 to 32,000 bases [1]. Most of these RNA viruses are prone to mutations [2,3]. Moreover, RNA viruses have a higher mutation rate compared to the DNA viruses, thereby, reflecting a higher replication fidelity of the DNA-dependent DNA polymerases over that of the RNA-dependent RNA polymerases [4]. Additionally, positive-sense single stranded RNA viruses, such as SARS-CoV-2, have a much higher mutation rate than the negative-sense single stranded RNA viruses [5]. The estimated rate of mutation reported is two per month for SARS-CoV-2 [6]. Mutation is also one of the primary generators of diversity among the genomes, including the viral genomes [6,7]. Thus, we are observing an emergence of variants of SARS-CoV-2 since the first incidence of the Coronavirus disease 2019 (COVID-19) [8].

Although SARS-CoV-2 originated in 2019, it has undergone roughly about 82062 mutations according to the GISAID database [9]. Particularly, mutation in the gene which encodes the Spike glycoprotein has been reported to be very high [10]. It is also well documented that those mutations which are found to affect the glycosylation of viral proteins affect the viral life-cycle [11]. Mutations at those residues which are used for recognition by antibodies make the virus resistant to antibody mediated neutralization [12]. In Spike protein, mutations can affect the transmission rate of the virus and also the disease outcome [13]. The first reported mutation of the Spike protein was D614G mutation, which was found to enhance the SARS-CoV-2 transmission [13]. The N501Y mutation increased the affinity of the Spike protein for its receptor, Angiotensin

Converting Enzyme 2 (ACE2), thereby increasing the chances of viral transmission [14]. Mutation E484K is known to contribute to the evasion of antibody neutralization [15]. D796H and H655Y mutations that are present in the Spike protein, are associated with reduced affinity towards the neutralizing antibodies [16]. The World Health Organization (WHO) has recently assigned different labels for the generated variants of SARS-CoV-2. They can be broadly separated into two categories, namely, the Variants of Concern (VOC) and the Variants of Interest (VOI) [17]. VOC has increased transmissibility and severity of (COVID-19) compared to VOI. Currently, there are four recognized VOCs; Alpha (B.1.1.7) estimated to be 40–80% more transmissible than the Wild-type SARS-CoV-2; Beta (B.1.351, B.1.351.2, B.1.351.3) has three mutations in the receptor-binding domain in the Spike glycoprotein of the virus: N501Y, K417N, and E484K respectively where, two of them (E484K and N501Y) mutate at the receptor-binding motif (RBM); Gamma (P.1, P.1.1, P.1.2) has about ten mutations in the Spike protein, where three mutations namely N501Y, E484K and K417T are of particular concern; and Delta (B.1.617.2, AY.1, AY.2, AY.3) where mutations occur at RBD regions T478K, P681R and L452R. This variant is of particular interest because it evades the neutralizing antibodies and also induces higher cell-cell fusion in the respiratory tract, contributing to the chances of higher pathogenicity [18].

The SARS-CoV-2 has several structural and non-structural proteins which assist the virus from initial attachment, entry to replication and other vital functions [18,19]. One of the largest and prominent structural proteins of SARS-CoV-2 is the Spike protein. This protein lies on the external viral membrane and helps in initial attachment of the virus with the host receptors [19]. Surprisingly, all the mutations that were observed in the VOC were primarily located in the RBD

ranging from residue 333-527 of the Spike protein [20]. The RBD of the SARS-CoV-2 Spike protein interacts with a human ACE2 receptor. This receptor is found on the lung alveolar epithelial cells and plays a primary role in protection against lung injury in humans [21]. Several studies have shown that the difference in the sequence of RBD between SARS-CoV-1 and SARS-CoV-2 have increased the binding affinity of the SARS-CoV-2 RBD towards ACE2 [22]. It is therefore essential to learn how these mutations impact the association of the RBD with the ACE2.

Very recently, the cryo-EM structure of the Delta Variant has been solved [23], however, the differences in structures and binding are yet to be unraveled. In the present study, we used molecular modelling tools to model the RBD domains of all the reported VOCs. Subsequently, we compared the generated models of the VOCs in the RBD/ACE2 complex with the Wild-type by using extensive molecular dynamics (MD) simulations and identified several key features which result in differential activity of the VOCs. This study provides mechanistic and molecular insights of the VOCs and would prove crucial for understanding the structure-function relationship as well as in the development of effective therapeutic strategies for the emerging variants of SARS-CoV-2.

Materials and Methods

Protein systems and setup

The crystal structure of the Spike protein RBD associated with ACE2 was taken from Protein Data Bank (PDB ID: 6LZG) as the starting structure [24]. The RBD has residues ranging from Tyr333 to Pro527. Although 13 residues were missing from the N-terminal of ACE2, the N-terminal

residues do not directly interact with the RBD [24,25], hence they were not modelled. This structure was considered as the Wild-type system. The variants namely, P.1(Alpha), B.1.1.7(Gamma), B.1.351(Beta) and B.1.167.2 (Delta) were generated by mutating specific residues in Wild-type Spike protein after aligning the RBD sequences shown in Figure S1. Modeller 10.1 molecular modelling suite was used to generate the new models based on the Wild-type RBD/ACE2 template [26]. To understand the effect of mutations on the structure and dynamics of the Spike-ACE2 complex, we performed all-atom MD simulations of Wild-type (WT) and four variants of Spike-RBD/ACE2. We also checked the initial structures of the generated variants by observing the distribution of their phi-psi angles and other stereochemical properties by using the PROCHECK [27] suite of programs.

Molecular Dynamics Simulations

Atomistic MD Simulation was carried out using Gromacs MD Simulation package [28] using CHARMM36 force field parameters [29]. Each system was subjected to energy minimization in steepest descent and then in conjugate gradient for 2000 steps. After initial relaxation, a cubic simulation box consisting of three-site TIP3P water molecules and neutralizing ions was created for the systems [30]. The box dimensions were 10 x 10 x 10 Å. For charge neutralization 24 ions were randomly placed by replacing the corresponding solvent molecules. Subsequently, energy minimization and thermalization was performed to avoid any bad contacts which might have been created due to the mutations and addition of water and ions. Periodic boundary condition was implemented during simulation. The systems were gradually heated from 0 to 310 K for 200 ps. Then the systems were equilibrated at 310 K in NVT ensemble using modified Berendsen

thermostat [31] for about 500ps and then equilibrated in NPT ensemble using 1 atmospheric pressure using Parrinello-Rahman barostat [31] for 1 ns. A time step of 2 fs was used for all the equilibration and subsequent production runs. After the convergence of potential energy and density, production simulation was carried out for the Wild-type and VOCs for 100 ns in NPT where the coordinates were saved at the interval of every 1000 ps. Particle-mesh Ewald method was used to treat the long-range electrostatic interactions [32]. VMD and Pymol were used for visualization of the trajectories [33,34]. All the analyses were carried out using Gromacs tools [35].

Binding energy calculation between RBD and ACE2

The binding energy between RBD and ACE2 for WT and VOCs (P.1, B.1.1.7, B.1.351 and B.1.167.2) were computed by using the Molecular Mechanics/ Poisson Boltzmann Surface Area (MM/PBSA) employed in the g_mmpbsa tool of GROMACS [36]. In this methodology, the binding energy of the target-ligand or protein-protein is typically defined as

$$\Delta G_{binding} = \Delta G_{complex} - (\Delta G_{protein} + \Delta G_{ligand})$$

where $\Delta G_{protein}$, $\Delta G_{complex}$, and ΔG_{ligand} represent the total free energies of the complex, the ligand, and the protein also separately in the solvent, respectively. Further, the free energy of the separate entity is represented as

$$G = E_{MM} + G_{solvation} - TS$$

where E_{MM} stands for the average molecular mechanic's potential energy in the vacuum, $G_{solvation}$ denotes the free energy of solvation. TS stands for the entropic augmentation to the free energy in

a vacuum, here S and T denote the entropy and temperature, respectively. The E_{MM} consists of nonbonded and bonded terms, including torsion, bond angle and electrostatic (E_{elec}) and the Van der waal (E_{vdw}) interactions, respectively & the solvation free energy, $G_{solvation}$ takes both electrostatic and non-electrostatic (G_{polar} and $G_{nonpolar}$) components. The binding free energy for the complexes was calculated from 50 snapshots over the last 10 ns of the simulation trajectories. All the systems were stable during this period.

Contact analysis

To understand the intermolecular interactions formed between RBD and ACE2 for WT and all the VOCs, contacts (hydrogen bonds and salt bridges) were computed and analyzed from the last 10 ns MD simulated trajectories using GetContacts [37]. The hydrogen bonds were shown in a clustergram to make the interpretation clear for visualization.

Results and Discussion

A. Modeling and simulation of Wild-type and VOC's RBD/ACE2 complex

The initial coordinates of the RBD/ACE2 complex were taken from the crystal structure (PDB ID: 6LZG) [24]. As shown in Figure 1 and Figure S1, the mutations of the VOCs occur at specific sites on the RBD of the Spike protein. Due to the unavailability of structural information of all the variants during the beginning of our study, we used Modeler10.1 molecular modeling suite [26] to generate four energetically stable structures RBD/ACE2 complexes where the corresponding amino acids (Figure 1a) were substituted to create initial conformations of the RBD variants (Figure 1b). The stability of the structures was verified through the DOPE score of Modeller10.1

(data not shown). Very recently, the structure of the B.1.167.2 has been deposited in the protein data bank (PDB ID: 7V8B) [23]. We have made a comparison between the structures generated after simulation with that of the Cryo-EM structure in the later parts of the article. The Ramachandran plot of the generated models did not show drastic changes as expected from a static model (Figure S3). Notably, these mutations were found to occur close to the RBD/ACE2 interface. It is therefore fascinating to investigate how Spike-ACE2 interaction and dynamics might be affected due to mutations.

To begin with, we ran atomistic MD simulations for WT, B.1.1.7, B.1.351, P.1 and B.1.617.2 variants for 100 ns at normal temperature and pressure (NPT) conditions. Figure S2 shows the root mean square deviation (RMSD) of the five systems calculated over the simulation run time. From the figure it is evident that P.1 and B.1.351 variants show a high RMSD value in comparison to the WT, however, the B.1.1.7 and B.1.617.2 RBD/ACE2 complexes have similar RMSD values. All the systems were found to be stable around 50ns of the run time. The RMSD of the systems during the last 20 ns of the run time lie within the range of 0.3-0.35 nm indicating that all systems have reached stability.

Once the systems reached stability, we further analyzed the fluctuations of the Cα atoms of the RBD and ACE2 proteins separately. Figure 2a shows the Root Mean Square Fluctuation (RMSF) of ACE2 protein. The ACE2 protein mainly plays a role in the cardiovascular system and in lungs, however its presence is also seen in other organs [38]. Further reviews on its role in various metabolic pathways are described elsewhere [39]. Structurally, ACE2 is an alpha helical protein

[40], where the crystal structure and our models that used the crystal structure as template, contain residues ranging from 19-615 of the ACE2 protein. The N-terminal helical part of the protein is the primary site of interaction with the RBD of the Spike protein of SARS-CoV-2. The overall binding mode of ACE2 with SARS-CoV-1 and SARS-CoV-2 is known to be largely similar [40,41]. The WT RBD shows that the N-terminal domain along with residues Glu329, Asn330 and Lys353 are mainly involved in building H-bonded/salt bridge interactions between the proteins (Figure 2a). In comparison with the WT from Figure 2a, we can clearly observe that fluctuations at the N-terminal region as well as the Glu329, Asn330 and Lys35 residues exists for B.1.351 and P.1 complex very prominently, however, ACE2 receptor in B.1.1.7 and B.1.167.2 show overlapping fluctuations with WT protein. We also compared the dynamics of the RBD in all the systems, where slightly higher peaks were observed for P.1 and B.1.351, but B.1.1.7 and B.1.167.2 systems were remarkably stable. The RBD of Spike protein contains a Receptor Binding Motif (RBM) which makes direct contacts with the ACE2 receptor [41]. The residues 438-506 comprise of RBM and are present towards the C-terminal of the RBD in our systems [42] (Figure 2b). As is evident from Figure 2b the fluctuations around this region remain overall similar, however marginally higher peaks were observed for B.1.351 and P.1. It is generally expected that mutations at residue level would alter the protein dynamics, however, even though mutations exist in B.1.167.2 and B.1.1.7, the RMS fluctuations were not much affected.

B. Difference in structure and dynamics of the VOC's

Figure 3 shows the time-averaged structures of the variants superimposed on the WT ACE2 receptor, to verify the relative orientation of the RBD with respect to ACE2. The interface formed

by the N-terminal helices of ACE2 and RBD were compared among the systems. From the figure we observed that the interface loop region of RBD and helices of ACE2 in the P.1 complex has moved further away when compared to WT (Figure 3a). On the other hand, B.1.1.7 superposes very well with the WT (Figure 3b). B.1.351 as well as B.1.167.2, however, appear to have moved closer to the ACE2 complex (Figure 3c, d). Subsequently, we analyzed the overall RBD/ACE2 complex after superimposition. Here, we found that although the orientation of RBD in P.1 and B.1.1.7 complexes were similar (Figure 3e, f), interestingly, B.1.351 as well as B.1.167.2 show a stark difference in the orientation of RBD (Figure g, h). In both the complexes we observed a relative rotation of the RBD w.r.t. ACE2. This significant shift in the protein orientation would influence its dynamics as well as residue positions and interactions in the protein-protein complex. To elucidate the change in the dynamics of the protein, we used Principal Component Analysis (PCA) on the generated trajectories and studied the dynamics of the RBD with respect to the ACE2 receptor.

PCA captures the dominant motions of the protein by using a set of eigenvectors. The most significant motion of a protein can be captured with the eigenvector with the maximum eigenvalue. For analysis, the PCA was performed on the backbone Cα atoms of RBD and ACE2 separately [43]. Figure S4 shows the comparison of motion of the proteins along the first principal components where we could observe potential protein dynamics. From Figure S4 it is evident that WT, B.1.351 and B.1.167.2 have similar protein dynamics, while P.1 and B.1.1.7 occupy a completely different cluster. This contrasts with the earlier observations in the time-averaged structure, where we found similarity between P.1, B.1.1.7 with WT. The Gibbs Free energy

landscape was then constructed as a function of the PC1 and PC2 coordinates. The highly stable protein conformation is shown in red, other low energy states are colored either in blue, green, or cyan. In the WT complex, the ACE2 was confined to a single cluster whereas, RBD explored two separate clusters (Figure 4a). This indicates that RBD can exist in two different conformations after being bound to ACE2. Although not much changes could be seen in the binding of RBD, the difference in clusters can be mainly attributed to the loop dynamics (Figure 4f). When we compared the variants, we found that a greater number of conformational states of the ACE2 in variants P.1 and B.1.351(Figure 4b, d), however, the ACE2 receptor of B.1.1.7 and B.1.167.2 explored the same low energy conformations (Figure 4c, e). This is expected since the mutations have primarily taken place in the RBD, which is devoid of large portions of the Spike protein. Moreover, despite the amino acid substitutions, the dynamics of the ACE2 receptor doesn't get influenced significantly. Later, we observed the dynamics of the RBD domain, which is the prime site of variation. Although the RBD of all the systems explored two different clusters, P.1 and more prominently B.1.1.7 show remarkable differences in the protein dynamics (Figure 4b, c). While, P.1 shows a single cluster with the low energy state of the protein, in B.1.1.7 the two different clusters are relatively shallow with more scattered low energy states. Surprisingly, despite observing significant changes in the superposed structures (Figure 3), the dynamics of B.1.315 and B.1.167.2 of both RBD and ACE2 were similar to the WT complex (Figure 4a, d, e). Thus, overall, our results reveal stark similarity in the dynamics of the RBD/ACE2 complex between WT, B.1.351 and B.1.162.7, but P.1 and B.1.1.7 show differences in the energetically stable states. We also checked for the trace values from the covariance matrix that was generated from the PCA. The trace values are correlated with the total variance in the values of eigenvectors where higher

values indicate more variation [44]. For ACE2 in WT, P.1, B.1.1.7, B.1.351 and B.1.162.7 the values were found to be 6.34 nm^2, 6.61 nm^2, 6.08 nm^2, 6.09 nm^2 and 5.98 nm^2 respectively. Similarly, for RBD it was found to be 1.02nm^2, 1.16 nm^2, 1 nm^2, 1.08 nm^2 and 0.97 nm^2 respectively. Thus overall, the maximum flexibility was observed for the P.1 complex in both ACE2 and RBD and the B.1.167.2 had the least flexibility among all the systems under study. This indicates that the B.1.167.2 was rather a tightly bound complex when compared to the other systems including the WT. Thus, we checked for the total binding energies of RBD/ACE2 in all the systems.

To explore the rationale behind the differential dynamics, we used the MM/PBSA to calculate the total binding energies of the protein complexes (Table 1). We used the last 10 ns of simulated trajectories of all the systems for MM/PBSA based binding energy calculations, where the systems were mostly stable. Table 1 shows the trend of the binding energies of the five systems under study. Accordingly, it is observed that the binding of B.1.167.2>P.1>B.1.351>WT>B.1.1.7. Upon comparison of the binding energies, we find B.1.167.2 to have the highest interaction energy and B.1.1.7 has the least. We also see large changes in the electrostatic interactions among the different complexes. Although there is an increase in electrostatic interaction energy which mainly accounts for the rise in the total binding energy of P.1, an increase in the polar solvation energy indicates higher solvent interaction of the protein, which is in accordance with the changes observed in Figure 3a. Similarly, B.1.1.7 shows a significant increase in the solvent accessible surface area (SASA) energy, which hints towards the difference of the accessibility of the protein to the solvent. An increase in the SASA value here indicates conformational change in the RBD/ACE2 complex.

From the table (Table 1), it is evident that B.1.351 and B.1.167.2 are more compact when compared to other complexes which are similar to the trace values observed in PCA. Thus, it was seen that the binding energies of B.1.167.2 is the highest and B.1.1.7 the least among all the five systems under study.

C. Interfacial residues significantly influence the stability of the RBD/ACE2 complex

Interfacial residues of proteins play a significant role in the association as well as in governing stability of the protein complexes. In the earlier studies by Spinello et al., [45] they compared the interface of SARS-CoV-1 with SARS-CoV-2 and found substantial differences in the interaction energies between residues of ACE2 and RBD. Here, we further calculated residue-wise contribution towards the total binding energy of the complex for both ACE2 and RBD by using MM/PBSA. Several of the residues were found to show drastic differences in their binding energies. We compared the energy of those residues that contributed >10 kJ/mol towards the binding energy of the complex. The interaction energies of RBD show radical changes in values for the P.1 complex. Here, almost all of the residues, except Glu484, contribute negligibly towards protein binding (Figure 5a). We further noticed that E484 mutates into K484 in both P.1 and B.1.351 which increases the binding energy to -226.64+/-2.8 and -258.40+/-4.71 kJ/mol respectively. However, E484 in the WT and B.1.1.7 show highly repulsive energy values (212.50+/-1.1 and 199.02+/-0.84 kJ/mol respectively) indicating unfavorable interaction. Similarly, substitutions L452R and T478K in B.1.167.2 significantly increase the interaction energies by -199.57+/- 0.57 kJ/mol and -186.29 kJ/mol. Overall, it was found that five residues in

B.1.167.2 and B.1.351, four in WT and B.1.1.7 contribute the maximum in the binding of RBD to ACE2.

Subsequently, we checked if complementary changes take place in the ACE2 receptor of the complexes. Upon comparing the interaction energy of the ACE2 protein residues with RBD, calculated from the last 10ns of the trajectory (Figure 5b), we found that in the WT complex except for residues D38, Y41, Y83, K31, D30 and T27, nearly all other residues show lower binding energies as compared to the VOCs. This indicates that mutations in the RBD impact the binding efficiency of ACE2 protein. Again, it was found that the residues of the B.1.1.7 variant show lower binding energies when compared to other variants. In P.1 majority of energy was found to be contributed by charged-hydrophilic Glutamate and Aspartate residues, i.e., E22, E23, D30, E35, D38, E56, E57, D67 and E75. However, the complementary binding was absent in the RBD which reduces the overall binding efficiency. Both B.1.351 and B.1.167.2 ACE2 interfacial residues show significantly high energies of interaction, particularly around residues E22, E23, K31, E35, E37, D38, E56, E57, D67 and E75 in B.1.351 and E22, E23, D30, E35, E37, D38, E56, E57, D67 and E75 in B.1.167.2 (Figure 5). The mutations in B.1.351 and P.1 comprises both unfavorable and favorable interaction. The changes observed for the B.1.1.7 variant w.r.t WT was not very significant. However, the mutations at L452R and T478K of the B.1.617.2 tremendously contributed towards the interaction energy (around -386 kJ/mol) of RBD/ACE2.

We superimposed the time averaged structure of the variants on WT complex to understand the relative loss and gain of interactions as observed from the contacts and MM/PBSA analyses. From

Figure 6 we can clearly see that the residues from the RBD have moved farther away from ACE2 in the P.1 complex (Figure 6a), at a similar position in B.1.1.7 (Figure 6b) and closer in both B.1.351 (Figure 6c) and B.1.617.2. (Figure 6d) ACE2 residues (Figure S5) on the other hand lie more or less at a similar position. We proceeded to further validate our findings by constructing a map summarizing the probability of formation of salt bridges and hydrogen bonds among the five systems. For the analysis we considered the last 10ns of the stabilized trajectory. In two out of three complexes (i.e., P.1 and B.1.351) we didn't observe any salt bridges. However, the salt bridges between D30 of ACE2 with K417 of RBD were found to be consistently present in WT, B.1.167.2 and B.1.1.7 systems. This loss of interaction can be attributed to the mutation that occurs at residue K417 in both P.1 and B.1.351. We also checked for the difference in the H-bond interactions among the residues calculated over the last 10ns of the trajectory. Results show that most of the H-bond interactions reported in earlier studies [46,47] were conserved in WT. ACE2 residue Y83 interacts with N487 of RBD across all the systems. There was a loss of H-bond between D30 of ACE2 with K417 of RBD in P.1 and B.1.351 (Figure 7). We found P.1 complex to have the least number of H-bond contacts and WT and B.1.167.2 to have the most H-bonded interactions with 7 and 5 H-bonded interactions for more than 50% of the time respectively (Figure 7). The two H-bonds lost in B.1.167.2 were located at RBD residues Y505 and T500 with ACE2 residues D37 and E355 respectively (Figure 7). This change takes place due to the major conformational shift in RBD binding to ACE2 in the B.1.167.2 complex. B.1.1.7 and B.1.351 each have 4 H-bonds whose occupancy was more than 50% of the time (Figure 7). Very recently, the cryo-EM structure of the ACE2 bound RBD of the Delta variant was deposited in the Protein Data Bank. We made a comparison of the simulated structures with the Cryo-EM structure of the Delta

variant (B.1.162.7) having the PDB ID :7V8B [23]. The relative RMSD value was found to be only 1.7 Å which indicates similarity between both the structures (Figure S6). Thus, we observed that the interfacial residues, especially the mutated residues significantly contributed towards the stability of the RBD/ACE2 complex. In Delta variant B.1.167.2, this increase in the interaction energy leads to the formation of a compact RBD/ACE2 complex compared to the WT. This strong protein-protein interaction along with dynamics close to the WT complex makes B.1.167.2 one of the most tightly bound variants of SARS-CoV-2.

Summary and Conclusion

COVID-19 pandemic caused by SARS-CoV-2 has affected millions worldwide. The peculiarity of the RNA virus lies in its ability to frequently undergo genomic mutations. These mutations lead to formation of several variants of the virus some of which turn out to be more infectious than that of the parent virus. The WHO has identified four such variants as Variants of Concern or VOCs, namely Alpha, Beta, Gamma and Delta. These variants have an enhanced level of transmission or virulence can able to divert themselves from therapeutics. Although vaccines and antibodies have been developed against COVID-19, there is a constant effort to identify and tackle novel and emerging varieties of the virus. In such a condition, it becomes extremely important for us to understand the molecular level details of interaction of the variant with the host receptor.

In the present study, we have used molecular modelling tools to model the RBD domains of the Spike protein of SARS-CoV-2 bound to the human ACE2 receptor. We have generated the models of all the four reported VOCs. Subsequently, we compared the generated models in the

RBD/ACE2 complex with the WT system by atomistic simulations. Since each of these mutations occurred close to the RBD/ACE2 interface, it is very challenging to understand the structure and dynamics of the RBD/ACE2 complex in the WT and the VOCs. All the systems had reached stability (RMSDs lie within 0.3-0.35nm) within 50ns of the simulation time. RMSF of the backbone Cα atoms of the RBD and ACE2 proteins indicated that B.1.351 (Beta) and P.1 (Gamma) variants show the maximum residue level fluctuations. Thus, although it is expected that mutations might affect the protein dynamics, RMSF of B.1.1.7 (Alpha) and B.1.617.2 (Delta) were low.

The orientation of the RBD with respect to ACE2 was checked to observe any conformational changes that might take place due to mutation. It was seen that at the interface region Gamma moved away and both Beta and Delta moved closed towards the ACE2 receptor. This also shows that the interacting residues might be more closely associated in Beta and Delta systems. Surprisingly, substantial conformational changes could be observed in the overall binding mode of RBD in Beta and Delta after simulation, where we could observe relative rotation of RBD w.r.t ACE2. Protein dynamics of RBD relative to ACE2 using PCA show that Beta and Delta fluctuations correspond well with WT, however, there was change in the dynamics of both Gamma and Alpha. The Delta complex was also found to be the most compact system indicative of tighter complex binding. Furthermore, we also analyzed the binding energetics of RBD/ACE2 in all the systems. MM/PBSA analysis indicated drastic gain of interaction energy particularly in the Beta, Gamma and Delta. Although, in Gamma polar solvation energy also contributed significantly to the total interaction energy. Overall, it was observed that electrostatic interactions play a major role in the binding of the complexes.

Detailed residue level energetics revealed that the most prominent changes in interaction energies were seen particularly at the mutated residues. The mutations in Beta and Gamma were both a mix of unfavorable and favorable interaction. The changes observed for the Alpha variant w.r.t WT was not very significant. However, the mutations at L452R and T478K of the Delta variant increased the RBD/ACE2 interaction drastically (around -386 kJ/mol). This increase in the interaction energy resulted in the formation of a much tightly bound RBD/ACE2 complex compared to the WT. The strong interaction energy coupled with dynamics similar to the WT complex makes B.1.167.2 one of the most tightly bound variants of SARS-CoV-2. Comparison of the recently solved cryo-EM structure of the Delta (7V8B) revealed high structural similarities with the final time-averaged structures obtained after simulation. The high affinity of RBD and ACE2 is directly indicative of an increase in the viral pathogenicity. Therefore, the present study would prove extremely crucial for design and development of effective therapeutic strategies for the emerging variants of the virus.

References

1. Pal Mahendra, Berhanu Gemechu, Desalegn Chaltu, Kandi Venkataramana. Severe Acute Respiratory Syndrome Coronavirus-2 (SARS-CoV-2): An Update. *Cureus.* **2020,** 12(3): e7423. Published online 2020 Mar 26. DOI: 10.7759/cureus.7423

2. Carrasco-Hernandez R, Jácome Rodrigo, López Vidal Yolanda, Ponce de León Samuel. Are RNA Viruses Candidate Agents for the Next Global Pandemic? A Review. *ILAR Journal,* **2017**, 58, 343–358, DOI: https://doi.org/10.1093/ilar/ilx026.

3. Duffy S. Why are RNA virus mutation rates so damn high? *PLoS Biol.* **2018** 13;16(8): e 3000003. DOI: 10.1371/journal.pbio.3000003.

4. Pachetti Maria, Storici Paola, Masciovecchio Claudio. Emerging SARS-CoV-2 mutation hot spots include a novel RNA-dependent-RNA polymerase variant. *J Transl Med* **2020** 18,179. DOI: https://doi.org/10.1186/s12967-020-02344-6.

5. Schoeman, D., Fielding, B.C. Coronavirus envelope protein: current knowledge. *Virol J.* **2019,** *16*, 69. DOI: https://doi.org/10.1186/s12985-019-1182-0.

6. Harvey, William T. SARS-CoV-2 variants, Spike mutations and immune escape. Nat. Rev. Microbiol.**2021** 19, 409–424. DOI: https://doi.org/10.1038/ s41579-021-00573-0.

7. Brüssow H. COVID-19: emergence and mutational diversification of SARS-CoV-2. *Microb Biotechnol.* **2021,** 14(3):756-768. DOI: 10.1111/1751-7915.13800.

8. Hu, B., Guo, H., Zhou, P. *et al.* Characteristics of SARS-CoV-2 and COVID-19. *Nat Rev Microbiol,* **2021**, 19**,** 141–154. DOI: https://doi.org/10.1038/s41579-020-00459-7.

9. Korber B, Fischer WM, Gnanakaran S, et al. Tracking Changes in SARS-CoV-2 Spike: Evidence that D614G Increases Infectivity of the COVID-19 Virus. *Cell*. **2020**;182(4):812-827.e19. DOI:10.1016/j.cell.2020.06.043.

10. Zhang Lizhou, Jackson Cody B., Mou Huihui, Ojha Amrita, Peng Haiyong. SARS-CoV-2 Spike-protein D614G mutation increases virion Spike density and infectivity. *Nature Communications,* **2020.** 11, 6013. DOI: https://doi.org/10.1038/s41467-020-19808-4.

11. Li Qianqian, Wu Jiajing. The Impact of Mutations in SARS-CoV-2 Spike on Viral Infectivity and Antigenicity. *Cell,* **2020**. 182, 1284–1294. DOI: 10.1016/j.cell.2020.07.012.

12. Wang Pengfei, Nair Manoj S., Liu Lihong. Antibody resistance of SARS-CoV-2 variants B.1.351 and B.1.1.7. *Nature* **2021***,* 593, 130–135. DOI: https://doi.org/10.1038/s41586-021-03398-2.

13. Tzu-Jing Yang, Pei-Yu Yu, Yuan-Chih Chang, Shang-Te Danny Hsu. D614G mutation in the SARS-CoV-2 spike protein enhances viral fitness by desensitizing it to temperature-dependent denaturation. J. Biol. Chem. **2021.** 297,101238. DOI: https://doi.org/10.1016/j.jbc.2021.101238.

14. Alenquer Marta, Lousa Diana, Amorim, Maria João. Signatures in SARS-CoV-2 Spike protein conferring escape to neutralizing antibodies. *PLoS Pathog* **2021**. 17(8): e1009772. DOI: https://doi.org/10.1371/journal.ppat.1009772

15. Jangra Sonia, Krammer Florian, Stadlbauer Daniel. SARS-CoV-2 Spike E484K mutation reduces antibody neutralization. *The Lancet Microbe* **2021**. 2, E283-E284, DOI: https://doi.org/10.1016/ S2666-5247(21)00068-9.

16. Sk Ramiz Islam, Debasish Prusty, Soumen Kanti Manna. Structural basis of fitness of emerging SARS-COV-2 variants and considerations for screening, testing and surveillance strategy to contain their threat. *medRxiv preprint* **2021.** DOI: https://doi.org/10.1101/2021.01.28.21250666.

17. Otto SP, Day T, Arino J, et al. The origins and potential future of SARS-CoV-2 variants of concern in the evolving COVID-19 pandemic. *Curr Biol*. **2021**. 31(14):R918-R929. DOI:10.1016/j.cub.2021.06.049.

18. Taylor, P.C., Adams, A.C., Hufford, M.M. et al. Neutralizing monoclonal antibodies for treatment of COVID-19. *Nat Rev Immunol* **2021**. 21, 382–393. DOI: https://doi.org/10.1038/s41577-021-00542-x.

19. Huang Yuan, Chan Yang, Xin-feng Xu, Wei Xu, Shu-wen Liu. Structural and functional properties of SARS-CoV-2 Spikeprotein: potential antivirus drug development for COVID-19. *Acta Pharmacologica Sinica* **2020.** 41,1141–1149; DOI: https://doi.org/10.1038/s41401-020-0485-4.

20. Schrörs B, Riesgo-Ferreiro P, Sorn P, Gudimella R, Bukur T, Rösler T, et al. Large-scale analysis of SARS-CoV-2 spike-glycoprotein mutants demonstrates the need for continuous screening of virus isolates. *PLoS ONE* **2021**. 16(9), e0249254. DOI: https://doi.org/10.1371/journal.pone.0249254.

21. Samavati Lobelia, Uhal Bruce D. ACE2, Much More Than Just a Receptor for SARS-COV-2. *Front. Cell. Infect. Microbiol*., **2020.** DOI: https://doi.org/10.3389/fcimb.2020.00317.

22. Lan, J., Ge, J., Yu, J. et al. Structure of the SARS-CoV-2 Spike receptor-binding domain bound to the ACE2 receptor. *Nature* **2020**. 581, 215–220. DOI: https://doi.org/10.1038/s41586-020-2180-5.

23. Yang TJ, Yu PY, Chang YC, Hsu STD. Local refinement of SARS-CoV-2 S-Delta variant (B.1.617.2) RBD and Angiotensin-converting enzyme 2 (ACE2) ectodomain (To Be Published).

24. Wang Q, Zhang Y, Wu L, Niu S, Song C, Zhang Z, Lu G, Qiao C, Hu Y, Yuen KY, Wang Q, Zhou H, Yan J, Qi J. Structural and Functional Basis of SARS-CoV-2 Entry by Using Human ACE2. *Cell.* **2020**. 181(4):894-904.e9. DOI: 10.1016/j.cell.2020.03.045.

25. Yan R, Zhang Y, Li Y, Xia L, Guo Y, Zhou Q. Structural basis for the recognition of SARS-CoV-2 by full-length human ACE2. *Science.* **2020.** 367(6485):1444-1448. DOI: 10.1126/science.abb2762.

26. Webb B, Sali A. Comparative Protein Structure Modeling Using MODELLER. *Curr Protoc Bioinformatics.* **2016**. 20;54:5.6.1-5.6.37. DOI: 10.1002/cpbi.3.

27. Wlodawer A. Stereochemistry and Validation of Macromolecular Structures. *Methods Mol Biol.* **2017.** 1607:595-610. DOI: 10.1007/978-1-4939-7000-1_24.

28. M.Abraham, T.Murtola, R.Schulz et al. GROMACS: High performance molecular simulations through multi-level parallelism from laptops to supercomputers. *SoftwareX* **2015.** 1–2, 19-25. DOI: https://doi.org/10.1016/j.softx.2015.06.001.

29. B.R. Brooks, C.L. Brooks III, A.D. MacKerell, Jr., L. Nilsson, R.J. Petrella, B. Roux, Y. Won, G. Archontis, C. Bartels, S. Boresch, A. Caflisch, L. Caves, Q. Cui, A.R. Dinner, M. Feig, S. Fischer, J. Gao, M. Hodoscek, W. Im, K. Kuczera, T. Lazaridis, J. Ma, V. Ovchinnikov, E. Paci, R.W. Pastor, C.B. Post, J.Z. Pu, M. Schaefer, B. Tidor, R. M. Venable, H. L. Woodcock, X. Wu, W. Yang, D.M. York, and M. Karplus. CHARMM: The Biomolecular Simulation Program. *J Comput Chem*. **2009**. 30(10):1545-614. DOI: 10.1002/jcc.21287.

30. A. D. MacKerell, D. Bashford, M. Bellott, R. L. Dunbrack, J. D. Evanseck, M. J. Field, S. Fischer, J. Gao, H. Guo, S. Ha, D. Joseph-McCarthy, L. Kuchnir, K. Kuczera, F. T. K. Lau, C. Mattos, S. Michnick, T. Ngo, D. T. Nguyen, B. Prodhom, W. E. Reiher, B. Roux, M. Schlenkrich, J. C. Smith, R. Stote, J. Straub, M. Watanabe, J. Wiórkiewicz-Kuczera, D. Yin, and M. Karplus. All-Atom Empirical Potential for Molecular Modeling and Dynamics Studies of Proteins. *J Phys Chem B* **1998** *102* (18), 3586-3616. DOI: 10.1021/jp973084f.

31. A. D. MacKerell, D. Bashford, M. Bellott, R. L. Dunbrack, J. D. Evanseck, M. J. Field, S. Fischer, J. Gao, H. Guo, S. Ha, D. Joseph-McCarthy, L. Kuchnir, K. Kuczera, F. T. K. Lau, C. Mattos, S. Michnick, T. Ngo, D. T. Nguyen, B. Prodhom, W. E. Reiher, B. Roux, M. Schlenkrich, J. C. Smith, R. Stote, J. Straub, M. Watanabe, J. Wiórkiewicz-Kuczera, D. Yin, and M. Karplus. All-Atom Empirical Potential for Molecular Modeling and Dynamics Studies of Proteins. *J Phys Chem B*. **1998**. 102 (18), 3586-3616. DOI: 10.1021/jp973084f

32. Darden, T.; York, D.; Pedersen, L. Particle mesh Ewald: An N·log(N) method for Ewald sums in large systems. *J Phys Chem B* **1993.** 98, 10089– 10092. DOI: 10.1063/1.464397

33. Lilkova, E., et al. The PyMOL Molecular Graphics System, Version 2.0. (Schrödinger & LLC, 2015).

34. Humphrey W, Dalke A, Schulten K. VMD: visual molecular dynamics. *J Mol Graph*. **1996**. 14(1):33-8, 27-8. DOI: 10.1016/0263-7855(96)00018-5. PMID: 8744570.

35. Kuczera, D. Yin, and M. Karplus. All-Atom Empirical Potential for Molecular Modeling and Dynamics Studies of Proteins. *J Phys Chem B* **1998.** 102 (18), 3586-3616. DOI: 10.1021/jp973084f.

36. Kumari R, Kumar R; Open Source Drug Discovery Consortium, Lynn A. g_mmpbsa--a GROMACS tool for high-throughput MM-PBSA calculations. *J Chem Inf Model* **2014**. 54(7):1951-62. DOI: 10.1021/ci500020m.

37. A. J. Venkatakrishnan, Rasmus Fonseca, Anthony K. Ma, Scott A. Hollingsworth, Augustine Chemparathy, Daniel Hilger, Albert J. Kooistra, Ramin Ahmari, M. Madan Babu, Brian K. Kobilka, Ron O. Dror. Uncovering patterns of atomic interactions in static and dynamic structures of proteins. *bioRxiv* **2019**. DOI: https://doi.org/10.1101/840694.

38. Salamanna Francesca, Maglio Melania, Landini Maria Paola, Fini Milena. Body Localization of ACE-2: On the Trail of the Keyhole of SARS-CoV-2. *Front. Med*., **2020** DOI: https://doi.org/10.3389/fmed.2020.594495.

39. E. Levine, T. Hwa. Stochastic fluctuations in metabolic pathways. *Proceedings of the National Academy of Science,* **2007**. 104 (22) 9229-9229; DOI: 10.1073/pnas.06109871049229.

40. Ni, W., Yang, X., Yang, D. et al. Role of angiotensin-converting enzyme 2 (ACE2) in COVID-19. *Crit Care,* **2020**. 24, 422. DOI: https://doi.org/10.1186/s13054-020-03120-0.

41. Duan Liangwei, Zheng Qianqian, Zhang Hongxia, Niu Yuna, Lou Yunwei, Wang Hui. The SARS-CoV-2 Spike Glycoprotein Biosynthesis, Structure, Function, and Antigenicity: Implications for the Design of Spike-Based Vaccine Immunogens. *Frontiers in Immunology* **2020.** 11, 2593.DOI:10.3389/fimmu.2020.576622.

42. Dudas G, Hong SL, Potter BI, Calvignac-Spencer S, Niatou-Singa FS, Tombolomako TB, Fuh-Neba T, Vickos U, Ulrich M, Leendertz FH, Khan K, Huber C, Watts A, Olendraitė I, Snijder J, Wijnant KN, Bonvin AMJJ, Martres P, Behillil S, Ayouba A, Maidadi MF, Djomsi DM, Godwe C, Butel C, Šimaitis A, Gabrielaitė M, Katėnaitė M, Norvilas R, Raugaitė L, Koyaweda GW, Kandou JK, Jonikas R, Nasvytienė I, Žemeckienė Ž, Gečys D, Tamušauskaitė K, Norkienė M, Vasiliūnaitė E, Žiogienė D, Timinskas A, Šukys M, Šarauskas M, Alzbutas G, Aziza AA, Lusamaki EK, Cigolo JM, Mawete FM, Lofiko EL, Kingebeni PM, Tamfum JM, Belizaire MRD, Essomba RG, Assoumou MCO, Mboringong AB, Dieng AB, Juozapaitė D, Hosch S, Obama J, Ayekaba MO, Naumovas D, Pautienius A, Rafaï CD, Vitkauskienė A, Ugenskienė R, Gedvilaitė A, Čereškevičius D, Lesauskaitė V, Žemaitis L, Griškevičius L,

Baele G. Emergence and spread of SARS-CoV-2 lineage B.1.620 with variant of concern-like mutations and deletions. *Nat Commun*. **2021**. 12(1):5769. DOI: 10.1038/s41467-021-26055-8.

43. Jolliffe Ian T. and Cadima Jorge. Principal component analysis: a review and recent developments. *Phil. Trans. R. Soc* **2016** A.3742015020220150202. DOI: https://doi.org/10.1098/rsta.2015.0202.

44. Giuliani A. The application of principal component analysis to drug discovery and biomedical data. *Drug Discov Today*, **2017**. 22(7):1069-1076. DOI: 10.1016/j.drudis.2017.01.005.

45. Spinello Angelo, Saltalamacchia Andrea, Magistrato Alessandra. Is the Rigidity of SARS-CoV-2 Spike Receptor-Binding Motif the Hallmark for Its Enhanced Infectivity? Insights from All-Atom Simulations. *J. Phys. Chem. Lett.* **2020**. 11, 4785−4790.DOI: https://dx.doi.org/10.1021/acs.jpclett.0c01148.

46. Liu S, Huynh T, Stauft CB, Wang TT, Luan B. Structure-Function Analysis of Resistance to Bamlanivimab by SARS-CoV-2 Variants Kappa, Delta, and Lambda. *J Chem Inf Model*. **2021**. 61(10):5133–40. DOI: 10.1021/acs.jcim.1c01058.

47. Zhang, L., Cui, Z., Li, Q. *et al.* Ten emerging SARS-CoV-2 Spike variants exhibit variable infectivity, animal tropism, and antibody neutralization. *Commun Biol* **2021**. 4**,** 1196. DOI: https://doi.org/10.1038/s42003-021-02728-4

Acknowledgements

NM thanks MHRD Government of India for her Doctoral Scholarship. SLR thanks NIT Warangal for research seed grant (P1131) and National Energy Research Scientific Computing Center of the Ernest Orlando Lawrence Berkeley National Laboratory, a DOE Office of Science User Facility supported by the Office of Science of the U.S. Department of Energy under Contract No. DE-AC02-05CH11231 and the Extreme Science and Engineering Discovery Environment (XSEDE). We are grateful to the COVID-19 HPC Consortium for providing resources and helping researchers work for a noble cause.

Author Contribution

NM and SLR designed research; NM performed research; NM and AKP analyzed data; NM, SLR and AKP wrote the paper.

Additional Information

Supporting Information Available. Includes Figures S1-S6 and Table 1. This information is available free of charge *via* the internet

Competing Financial Interests

The authors declare no competing financial interests.

Figure Legend

Figure 1. (a) Superimposed structure of the WT and the Variants highlighting the mutations in RBD. Wild type ACE2 receptor is shown in magenta and RBD in green cartoons. The mutations are shown as sticks. (WT: green, P.1: red; B.1.1.7: Orange; B.1.351: blue; B.1.617.2: Cyan) (b) Sequence alignment of WT and the VOCs. Mutated residues are highlighted in red in the sequence

Figure 2. RMSF of (a) ACE2 and (b) RBD with respect to WT complex. In both ACE2 and RBD, the residues from B.1.1.7 and B.1.617.2 show more stability as well as similarity with the WT complex. The ACE2 residues participating in salt bridge formation in WT are shown by arrows. The RBD region is shown as cyan bar in (b), where the RBM is highlighted in orange.

Figure 3. Superimposed structure of WT and VOCs showing the relative variation in the receptor binding domains. Interfacial region of RBD and ACE2 in (a) P.1, (b) B.1.1.7, (c) B.1.351 and (d) B.1.167.2. When the structure is rotated 90° in (e) P.1, (f) B.1.1.7, (g) B.1.351 and (h) B.1.167.2. Relative displacement was observed in B.1.351 and B.1.167.2. (WT: RBD in cyan, ACE2 in pink; P.1 RBD in red; B.1.1.7 RBD in Green; B.1.351 RBD in Blue; B.1.167.2 RBD in Magenta).

Figure 4. Free energy landscape of the WT and VOCs. The Gibbs free energy landscape was constituted from the simulated structures on the plane defined by the first principal component of ACE2 and RBD in (a) WT, (b) P.1, (c) B.1.1.7, (d) B.1.351 and (e) B.1.167.2. The state with the

lowest energy is coloured in red. The two clusters formed by RBD are shown in green and magenta cartoons. The clusters are formed primarily due to loop dynamics.

Figure 5. Residue level contribution towards the interaction energy. Contribution of (a) RBD and (b) ACE2 for all the five systems under study. The mutated residues are highlighted by a *. Color code; WT- Cyan, P.1- orange, B.1.351-Yellow, B.1.1.7- Green and B.1.167.2- Brown.

Figure 6. RBD interfacial residues primarily participate in interaction with ACE2. Superimposed images of WT with (a) P.1, (b) B.1.1.7 (c) B.1.351 and (d) B.1.167.2. Color scheme: WT (cyan), P.1 (red), B.1.1.7 (green), B.1.351 (blue) and B.1.167.2 (magenta). Negative displacement was prominently seen in P.1 while B.1.351 and B.1.167.2 moved towards the ACE2 receptor.

Figure 7. Computed hydrogen bonds between RBD and ACE2 for WT and VOC complexes. The gradient of green shows the frequency of interactions in the last 10 ns MD simulation trajectories. The contacts were shown as clustergram to make the interpretation clear for visualization.

FIGURES

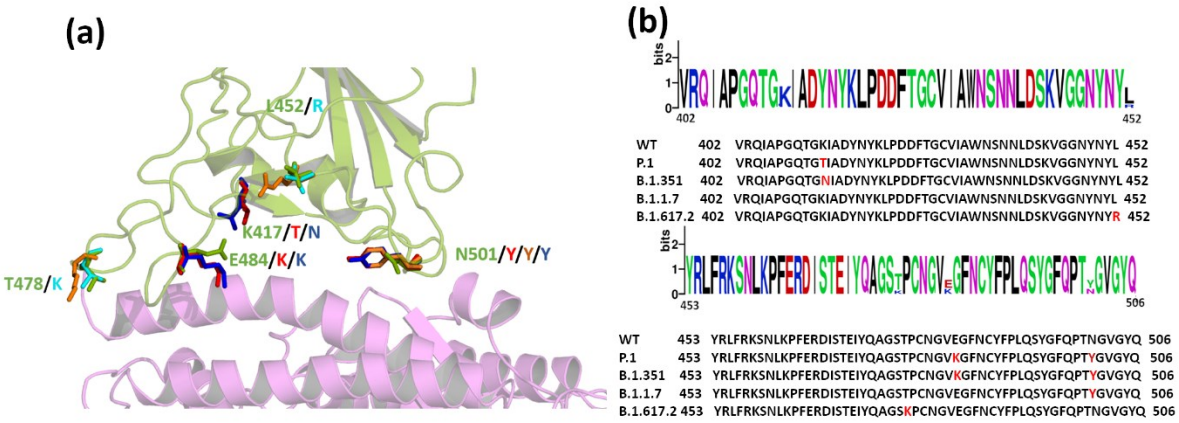

Figure 1.

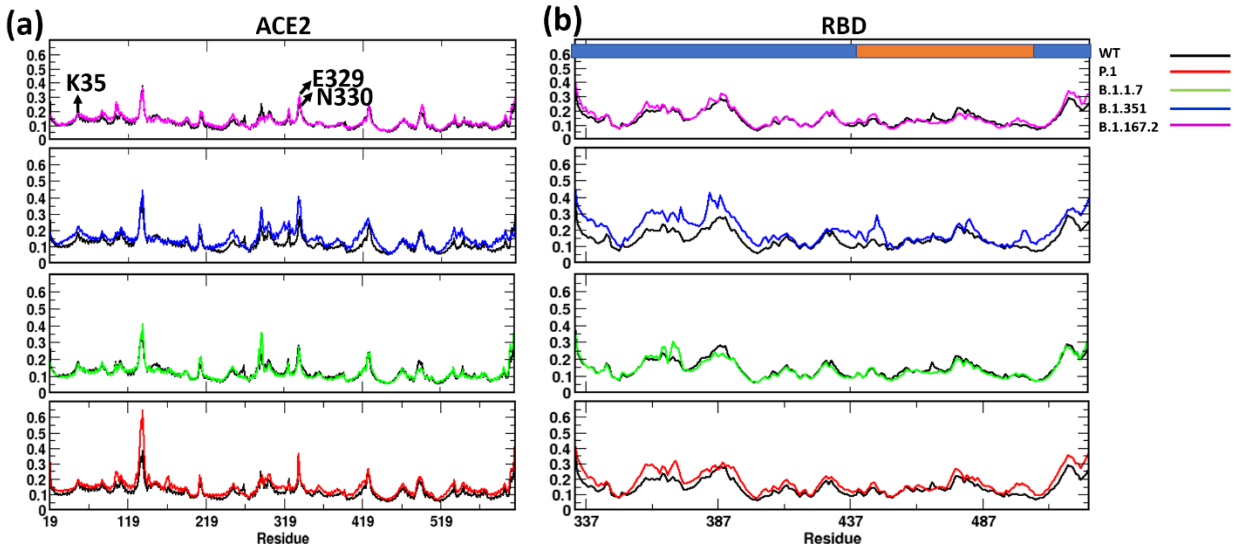

Figure 2

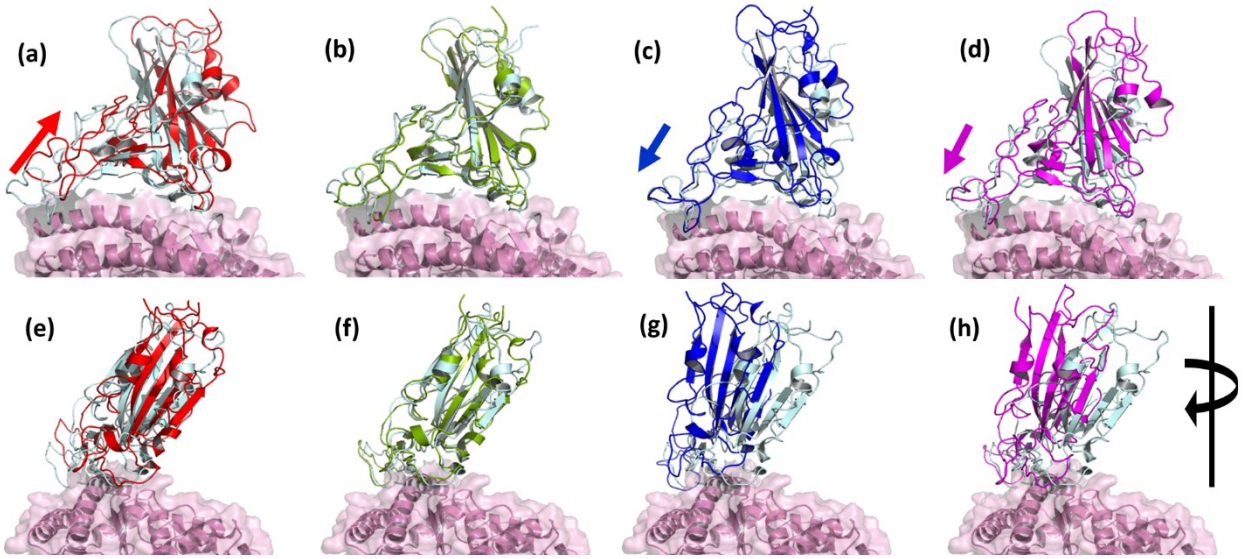

Figure 3.

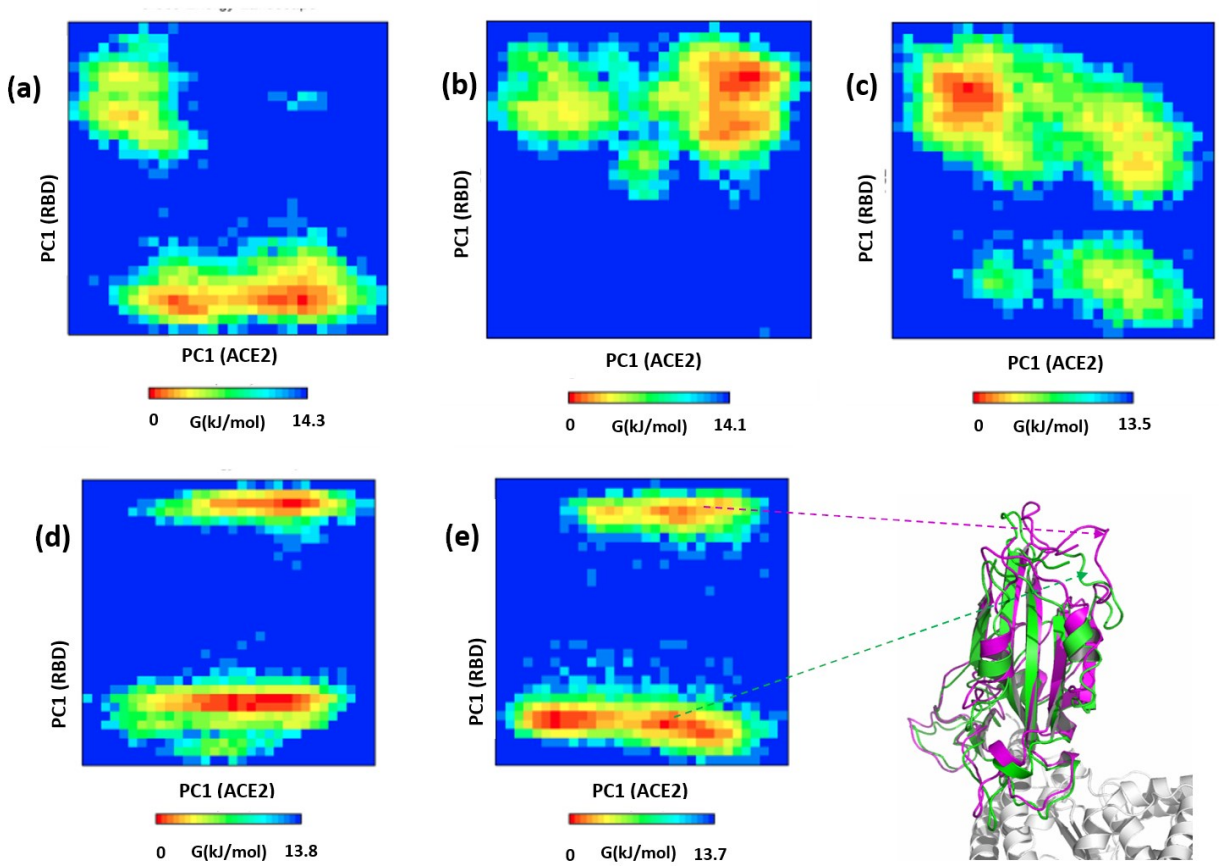

Figure 4.

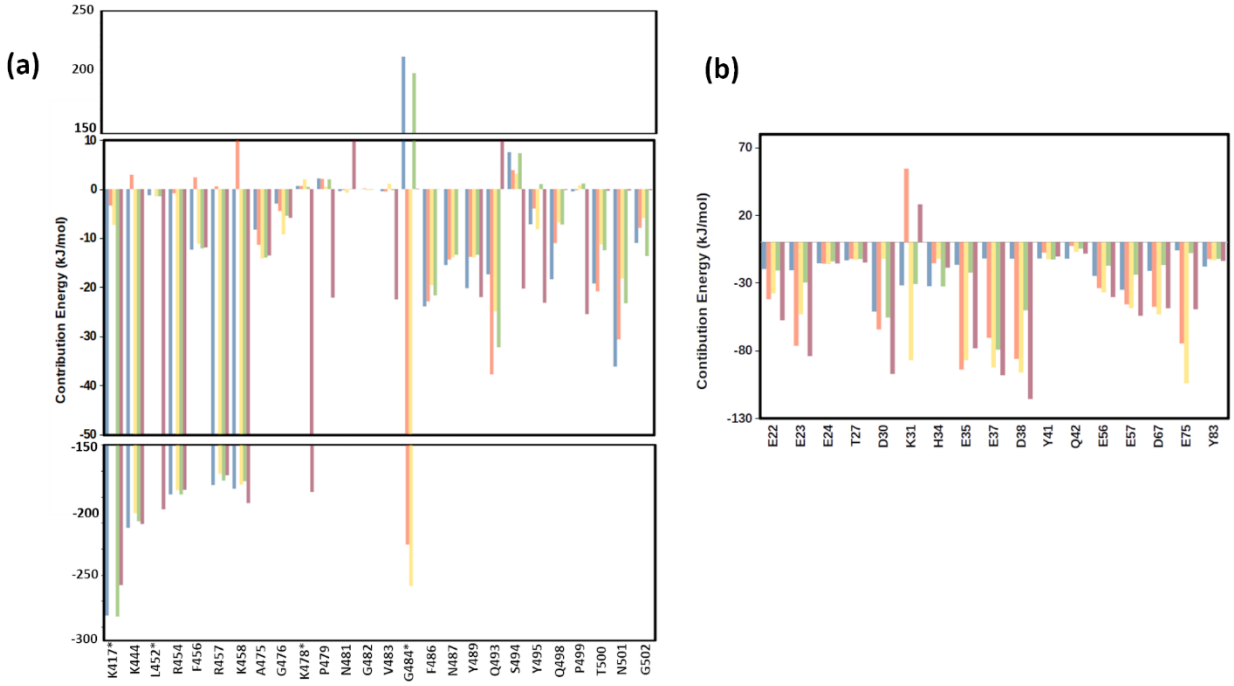

Figure 5.

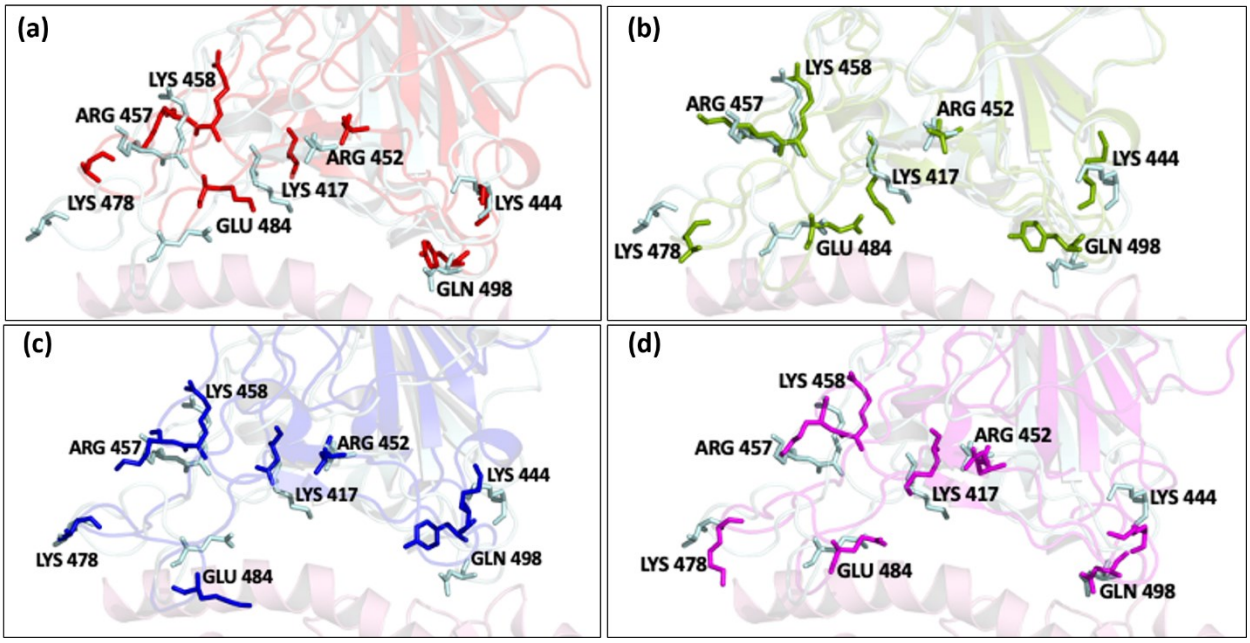

Figure 6.

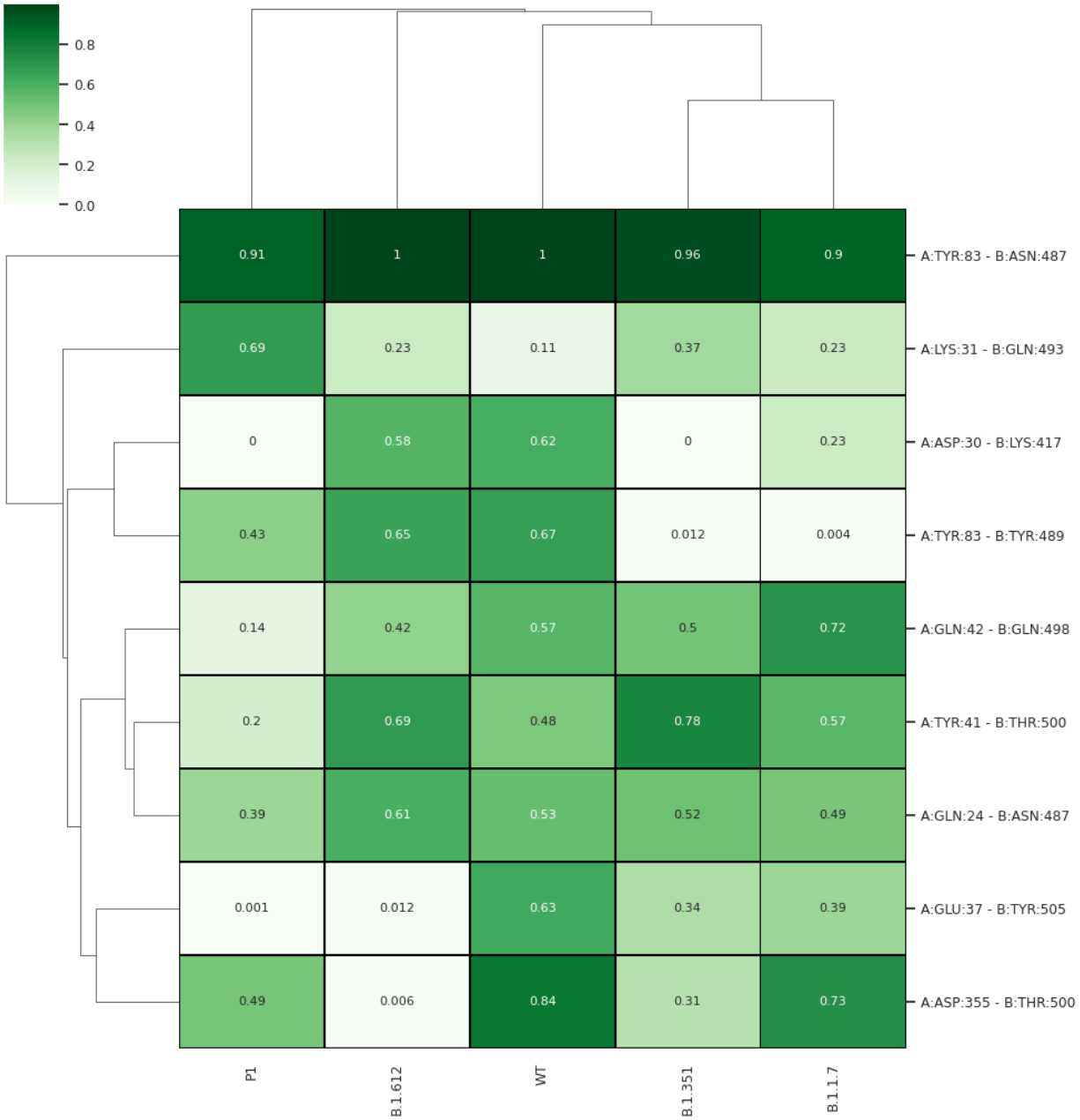

Figure 7.

Table 1. Interaction energies between RBD and ACE2 in WT and VOCs

List of VOCs	Van der Waal energy (kJ/mol)	Electrostatic energy (kJ/mol)	Polar solvation energy (kJ/mol)	SASA energy (kJ/mol)	Total Binding energy (kJ/mol)
WT	-363.775 ± 20.446	-1232.614 ± 64.543	617.810 ± 161.796	-43.889 ± 3.469	-1022.467 ± 150.703
P.1	-344.279 ± 22.058	-1628.128 ± 85.641	396.771 ± 168.090	-42.888 ± 4.565	-1618.525 ± 139.268
B.1.1.7	-334.114 ± 19.106	-1010.046 ± 69.032	509.951 ± 82.835	-74.747 ± 3.721	-908.956 ± 91.026
B.1.351	-282.277 ± 20.433	-1659.780 ± 108.968	539.401 ± 156.941	-36.157 ± 3.835	-1438.813 ± 140.383
B.1.167.2	-320.790 ± 20.134	-1985.424 ± 67.699	558.329 ± 109.035	-40.544 ± 3.624	-1788.429 ± 99.618